ASIAN JOURNAL OF CIVIL ENGINEERING (BHRC) VOL. 18, NO. 4(2017)
PAGES 577-592

EFFECT OF CONCRETE DECKS IN INCREASING STRENGTH AND STIFFNESS OF DOUBLE-LAYER GRIDS

A. Hosseinmardi[1] and M. Heristchian[2*]
[1]College of Graduate Studies, South Tehran Branch, Islamic Azad University, Tehran, Iran
[2]Department of Civil Engineering, South Tehran Branch, Islamic Azad University, Tehran, Iran

Received: 12 Sepember 2016; **Accepted:** 27 November 2016

ABSTRACT

This paper studies the increase in strength and stiffness of the composite double-layer grids, whose top-layers combine the steel frame elements with concrete decks. Firstly, the paper obtains the ultimate load capacities of square concrete decks with and without ribbed edges under various support and load conditions. Then, the load capacity of a composite double-layer grid is obtained under various loads, geometric and support conditions. A comparison of the results indicates that: the composite grid exhibits 2 to 5 times higher load capacity than the corresponding non-composite grid. In addition, a composite grid with (roller +pin) supports has about 20% of the load capacity of the identical grid with (pin +pin) supports.

Keywords: Concrete decks; double-layer grids; ultimate strength and stiffness; composite spatial structures; numerical modelling.

1. INTRODUCTION

The use of composite beams obtained by combining concrete decks with steel beams or plate girders is a common practice in construction of bridges and floors with heavy loads. Structural design codes provide rules for design of such composite floors. The codes specify the necessary and sufficient conditions for the composite action between steel and concrete. Yet for such decks, developing methods for quantifying the elasto-plastic cross-sectional behaviour of composite beams is required (for instance, Ban and Bradford, 2015 [1]).

Floors of multi-storey buildings, passenger terminals, car parks, shopping malls, grandstands for stadiums, stands for sports halls, pedestrian bridges, motorway bridges, and helipads are examples of constructions which in addition to sizable dead loads, bear heavy live loads. In a composite floor, not only concrete serves as the cladding material, but also it accompanies the steel sections in bearing the loads. The reinforced concrete slab together with

*E-mail address of the corresponding author: heris@azad.ac.ir (M. Heristchian)

the embedded top chord forms the top-layer of the space truss and resists the compressive forces, while the steel sections of bottom chord elements resist the flexural tensile forces. The mid-layer (web) steel elements carry the shear forces.

Similar to the one-way beams, one can combine two-way or three-way grids with concrete decks to construct composite grids. The composite grids (or spatial structures) can have one or more layers, and in general, they can have all variety of patterns available for single and /or multi-layer grids, such as 2-way, 3-way or honeycomb patterns.

Double-layer grids can offer efficient solutions for many constructional applications. Optimizing the design of double-layer grids will further increase their efficiency. Grigorian, 2013 and 2014 [2 to 4], use performance control and plastic design for efficient design and optimization of grids and parallel chord trusses (which can be used as the basic unit of two-way flexural grillages). Kaveh et al, 2011 [5], compared optimality of two configurations for double-layer grids. Also, Kaveh and Hassani, 2011 [6], used the energy concepts to deal with nonlinearities in optimum design of structures (as well as double-layer grids). Gholizadeh et al, 2013 [7] and [8] have worked on optimization of double-layer grids.

Many countries have used composite spatial structures for roofs and floors for over four decades. Lan, 1984 [9], (Shilin and Hengxi, 1993 [10]), (Liu, 2006 [11]), and (Dong and Zhao, 2006 [12]) report various aspects of composite constructions in China for roofs and floors and classify various types of spatial structures. In China, they have used double layer composite grids for roofs of the grids with span as large as 45mx58m.

El-Sheikh, 2000 [13], reported a double-layer grid with the ability to work compositely with concrete slabs. Schaad, 2005 [14], investigates open-web joists forming a two-way steel floor system.

Heristchian, 1990 [15], reports the details of the connection of concrete decks for a type of composite double-layer grid. This type of concrete deck (tray), with some alterations was employed for construction of floors for a number of shopping malls and grandstands of sports halls in Iran, during 1990's. The pedestrian, or motorway bridge designs of Schlaich and Bergemann, 2003 [16], indicate that composite constructions can provide economic and aesthetic bridge solutions. Strasky, 2007 [17], demonstrates a number of beautiful pedestrian bridge designs which utilise the tension and compression capacities of the structural members in a very efficient way, by combining appropriate steel and concrete elements.

Hong, 1984 [18], analytically and experimentally investigated the behaviour of two-way composite double-layer grids. Hong's experimental model used precast reinforced ribbed slabs. Thompson and Kubik, 1993[19], report the results of experimental and numerical work on a two-way flexural (Vierendeel type) grillage.

El-Sheikh and McConnel, 1993 [20], also El-Sheikh and El-Bakry, 1996 [21], carried out experiments on composite double-layer grids. They found that composite action improves the overall ductility of the grid. The attachment of timber boards or concrete slabs to the top-layer elements improves the structural characteristics and its cost effectiveness. In their tests, the timber boards increased 82% strength and 20% stiffness of grids. Also, addition of concrete slabs C20, with thickness 50mm increased 87% strength and 27% stiffness of the corresponding non-composite double-layer grids. The composite action could control the brittle behaviour of the spatial grids (El-sheikh, 1999 [22]). It also, eliminates the buckling of the top (compression) members. According to his studies, embedding of the concrete slab

within the top-chord elements eliminates the need for the additional shear connectors.

There are various methods for construction of composite double-layer grids. A method uses precast concrete panels (trays) to fill the open spaces of the top-layer of the double-layer grid. The cast in situ concrete needs considerable amount of formwork and scaffolding. However, the precast concrete panels exclude the need for expensive formwork and scaffolding. Fig. 1(c) shows positioning of the precast concrete panels over the top-chord elements of a double-layer grid. Here, the interconnection pattern of the double-layer grid is of the type 'obnate on larger obnate' [23]. This type of grid bears the name SDC grid, after the French architect and engineer, Stephen Du Chateau who used this type of double-layer grid for construction of many projects. The top-layer of the 'SDC' grid has a diagonal pattern, which normally requires triangular concrete panels at edges and corners.

Figure 1. (a) View of a precast concrete panel under load test, (b) The dial-gauge, and (c) The use of precast concrete panels in a composite double layer grid

Fig. 2, shows the details of the precast concrete panels of the samples built and shown in Fig. 1. The thickness of the concrete panel depends on the amount of the applied load and the size of the module. The present study assumes square units of diameter 1.5m. The square concrete panel has ribs along its four edges. The panel has the net plan dimensions 1048x1048 mm, and the thickness 35 mm. At the ribs the thickness increases to (35+65=) 100 mm. The plan size of the panel results in the gross diagonal size of 1500 mm. The top-right of Fig. 2, shows the reinforcement of the panel, which is T6 (rebar of diameter 6) at every ~100 mm in both directions, together with four T8 at top edges, and T14 at bottom of ribs. The reinforcements T6 extend outwards the concrete panels (as also, seen in Fig. 1). The inter-panel extended portions of the reinforcements are interwoven (section b-b of Fig. 2). Non-shrinkable grout fills up the gap between the concrete panels. Steel angles or T-profiles are suitable choices for the top-layer elements of the composite double-layer grids. One can use appropriate ½H profiles for making T-sections as well.

In a composite double-layer grid, a concrete panel is under the two-fold action of

(a) Local bending due to the gravitational load acting at each unit (panel) which is

investigated by analysis of a single panel under various load and support conditions.

(b) Overall compression due to the general bending of the double-layer grid with a simple span, which is studied by analysis of the composite double layer grid.

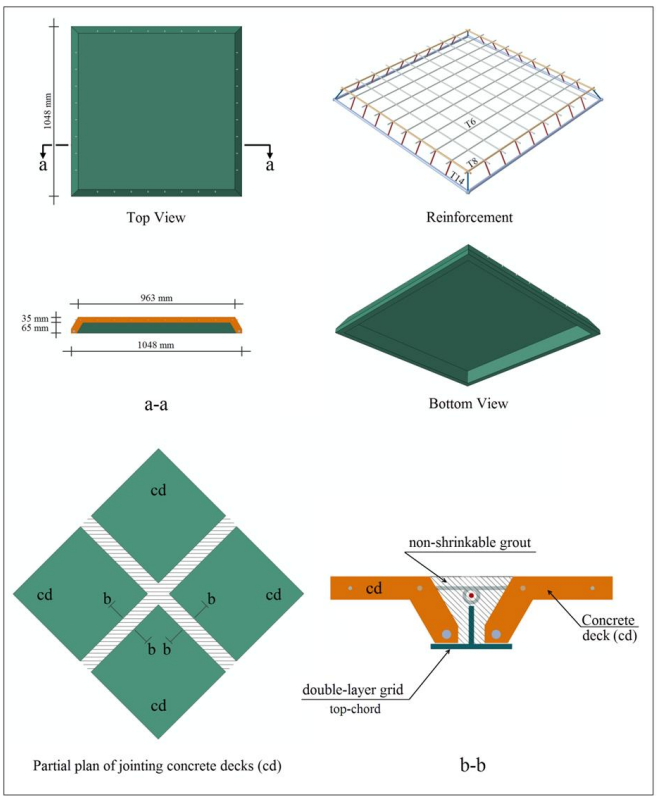

Figure 2. Geometry of the precast concrete deck (panel)

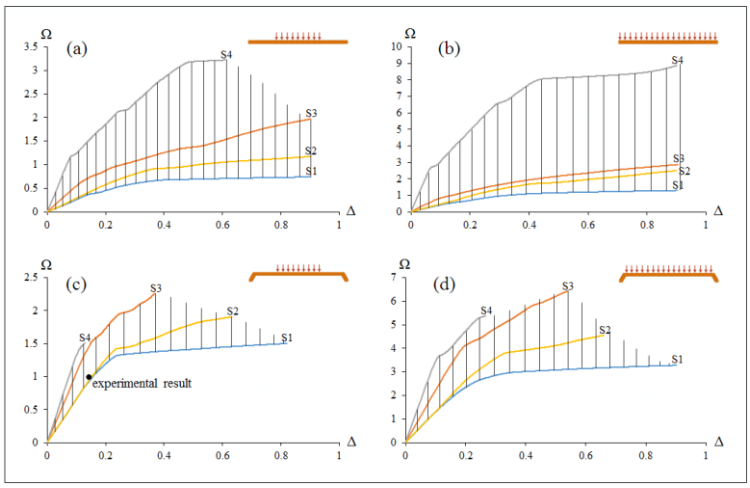

Figure 3. Load-displacement diagrams for concrete panels with various geometry, load and support conditions

2. BEHAVIOUR OF A SINGLE CONCRETE PANEL

Fig. 3, shows load-displacement diagrams for concrete decks under various geometry, load and support conditions. The vertical and the horizontal axis of the diagrams denote the load factor (Ω) and the displacement factor (Δ) of the panels. The common multiplier of the load factor (Ω) is P_0=9.8 kN, which is the amount of load for the experimental panel of Fig. 1 (The point indicated by a solid circle in Fig. 3(c)). The common multiplier of the displacement factor (Δ) is δ_0= (span/350=3mm). The parameters S1 to S4 of the diagrams denote the support conditions:

(i) S1, four simple supports at corners of the deck,

(ii) S2, four simple supports at corners plus four edge angles,

(iii) S3, four simple supports at corners plus horizontal (xy) supports at four edges,

(iv) S4, full (xyz) supports all around (at corners and edges) the concrete deck.

In addition, the top right part of each diagram of Fig. 3 schematically shows the geometry and loading of the concrete panel under various support conditions. Each panel has either a 'central' or a 'uniform' loading. The central load occupies the central (500 mm x 500 mm) area of deck (The left-hand diagrams (a) and (c)). This loading resembles the loading of Fig. 1(a). The uniform loading occupies completely the top surface of the deck (The right-hand diagrams (b) and (d)).

The diagrams 3(a) and (b) relate to flat concrete panels, whereas the diagrams 3(c) and 3(d) relate to edged (ribbed) panels. Among the four diagrams of Fig. 3, the support types S1 and S4, invariably, have the lowest and the highest strength, respectively, which demonstrates the natural character of increase of strength with the increase of confinement. A summary of the points regarding the diagrams of Fig. 3 is as follows:

- Under the support type S1, the ribbed deck has 2.5 to 4 times higher elastic stiffness than that of a flat deck under central and uniform loads, respectively.
- Support S1 has the largest ductility range among all the four support conditions.
- The full confinement of support conditions S4 moderates the difference between a flat and a ribbed deck. Nonetheless, in this case, the elastic stiffness of the uniform load is over twice larger than the stiffness of the central load.

The question is that which one of the support conditions S1 to S4 (or a combination thereof) occurs, for the concrete panels used as the top-layer of a double-layer grid. The prompt answer is that the type of support depends on the detailing of the connection of the concrete panel to the top-layer of the double-layer grid. Nonetheless, a profound and comprehensive answer to this question needs a good number of load tests on double-layer grids with both ribbed and flat pre-cast concrete decks. As Fig. 2 shows, the non-shrinkable grout filling the gap between the concrete decks, together with the web of the inverted T-section, confines the concrete panel against the horizontal movements. Thus, the separation of the concrete panel from the lattice elements of top-chord of the grid could not easily occur. Additionally, confining the in-plane displacement of the concrete panel develops the shear interaction. The slip strain at the steel and concrete interface defines the level of the composite action. A certain level of shear interaction prevents the relative slippage of the concrete panel and the surrounding top-chord elements and provides the ability of the

concrete panels to contribute to the composite action. The support conditions S1 and S4, correspond to the 'lower bound' and the 'upper bound' load capacity of the concrete panel, respectively. In this paper, the support type S3, with a confining degree less than S4, most likely defines the restraints for a concrete panel in a composite grid of the type under consideration.

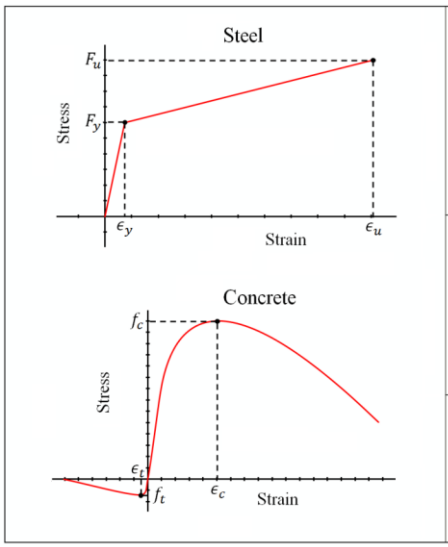

	property	value
Structural Steel Section	Young's Modulus, E_s	205 GPa
	Poisson's Ratio, ν	0.3
	Yield strength, F_y	240 MPa
	Ultimate strength, F_u	460 MPa
	Yield strain	11.7×10^{-4}
	Ultimate strain	24.6×10^{-2}
Reinforcement	Young's Modulus, E_s	205 GPa
	Poisson's Ratio, ν	0.3
	Yield strength, F_y	300 MPa
	Ultimate strength, F_u	500 MPa
	Yield strain	14.6×10^{-4}
	Ultimate strain	20.1×10^{-2}
Concrete	Young's Modulus, E_c	25.1 GPa
	Poisson's Ratio, ν	0.15
	Compressive strength, f_c	28 MPa
	Tensile strength, f_t	2.8 MPa
	Ultimate strain, ϵ_c	0.0032

Figure 4. The steel and concrete constitutive material properties

Fig. 4 shows the constitutive properties for steel and concrete. The structural steel sections and reinforcement for concrete both have bi-linear stress-strain diagrams, where the ultimate strain ε_u, corresponds to the ultimate strength of steel Fu. The concrete has a low capacity of 20MPa, which behaves differently in compression and tension (Park and Paulay, 1975 [24]). The tensile strength of concrete is about 0.1 of its compressive strength. For the numerical analysis of a single panel, 'solid', 'beam' and 'shell' elements are used to represent the concrete, reinforcement, and structural angles, respectively. The reinforcements are 'embedded' in concrete [25, 26]. Only the panel with support type S2 has structural angles that are in contact with concrete at four corners.

Fig. 3, represents normalised force-displacement diagrams for sixteen cases of analysis of concrete panels. Figs. 5 and 6, show snap shots of the results of analysis (for a quarter of a panel). The time of the snap shot is about the terminating (the final failure) points of the diagrams of Fig. 3. In Fig. 5 and 6, S1(a), S1(b),…, S4(d) stand for the respective cases of Fig. 3, for instance, S1(a) relates to the flat panel with support type S1 under the central load, and S4(d) stands to the edged panel with support type S4 under the uniform load. The crack indicator (PE), the maximum vertical deflection (U2), and the normal stress (S11) of the reinforcement and the supporting angles, have a common basis for support types S1 to S4, for both central and uniform loads. The main cracks for supports S1 or S2 (a, b), under central or uniform load occur along the lines joining the middle of the opposite sides of the panel, whereas, for the supports S3 and S4 (a, b), cracks occur nearby the four sides of the panels. The reinforcements of cases S1 and S2 (a, b) have almost twice of the maximum tensile

stresses of the panels with support types S3 and S4 (a, b).

Diagonal cracks appear for the edged panels, Fig. 6, with supports S1 and S2, under both central and uniform loadings (c, d). On the contrary, for the supports S3 and S4, the cracks occur nearby the four sides of the panels. Though for the case S4 (c), the cracks develop at the central parts of the sides to a length equal to about one-third of the side length and stop far short of the corners.

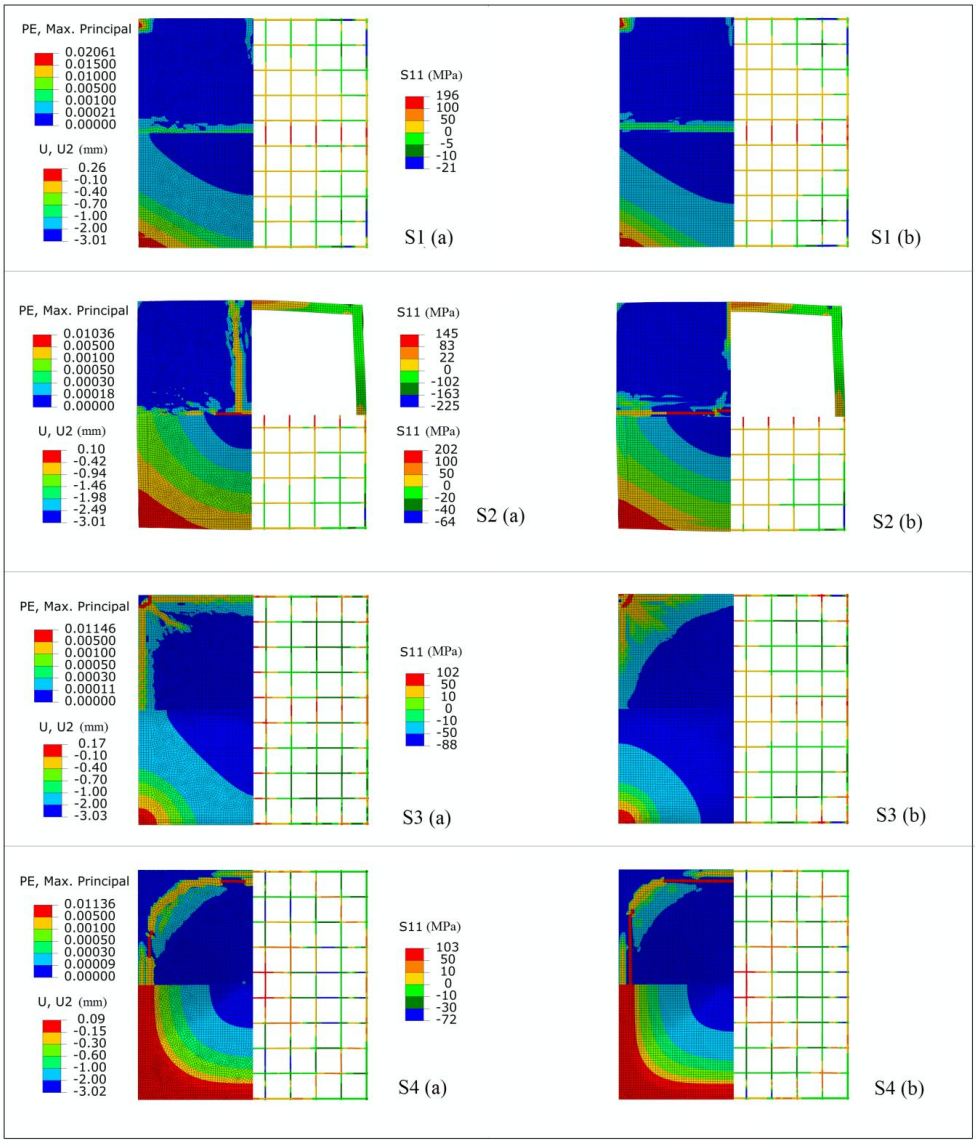

Figure 5. Results of analysis of flat panels under central (left) and uniform (right) loads, (PE) concrete cracks, (U2) vertical displacement, and (S11) stress of support angle and/or reinforcement

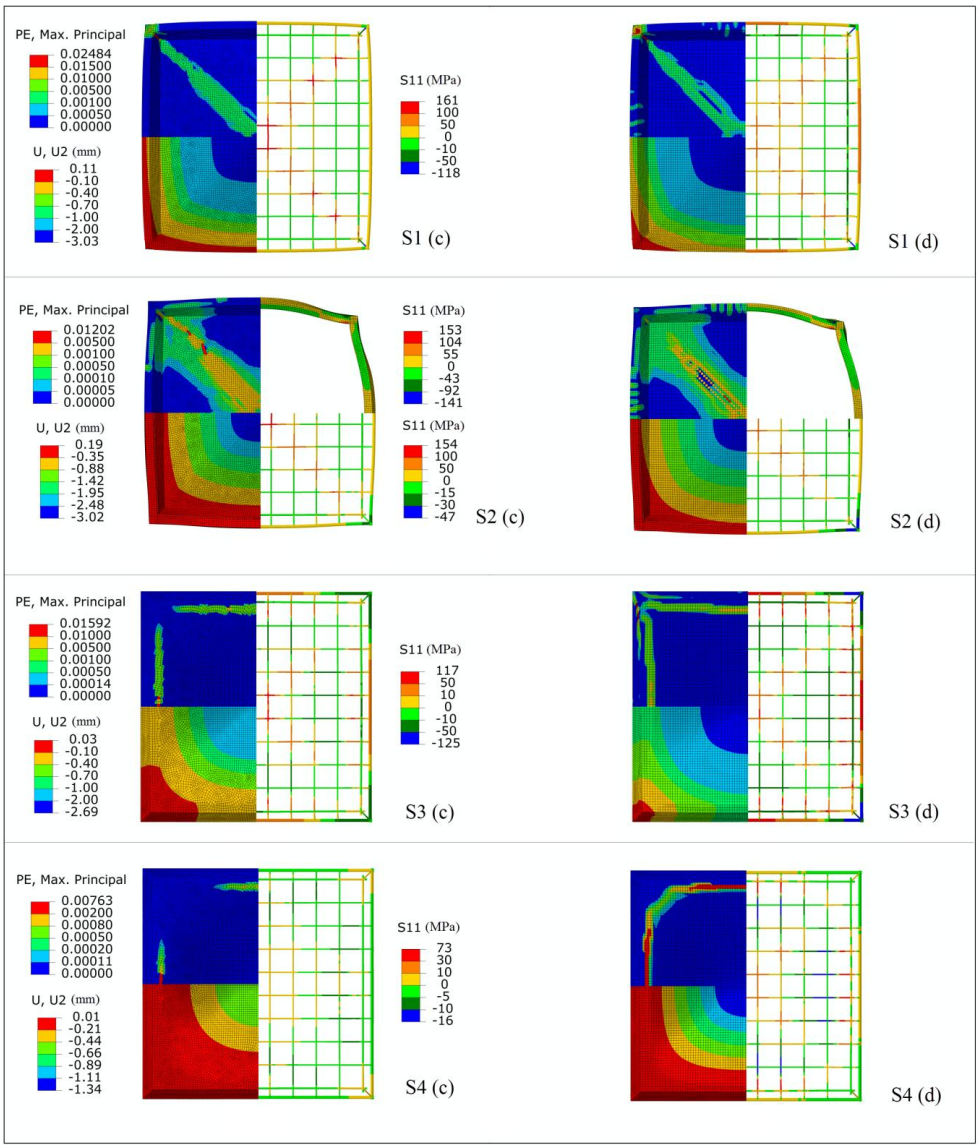

Figure 6. Results of analysis of edged panels under central (left) and uniform (right) loads, (PE) concrete cracks, (U2) vertical displacement, and (S11) stress of support angle and/or reinforcement

3. BEHAVIOUR OF A COMPOSITE DOUBLE LAYER GRID

In order to evaluate the range of increase in strength and stiffness due to the composite action, a composite double-layer grid of type SDC with overall dimensions 12m x 4.5m x 0.75 m of Fig. 7 is studied numerically under several conditions. The ribbed pre-cast concrete panels of size 1060 mm x 1060 mm (as of Fig. 2) are used in combination with the

top-chords of the grid. A non-shrinkable concrete-based grout (with a detail such as section b-b of Fig. 2) fills the gaps between the adjacent concrete panels. The internal and the edge-elements of the top-layer of the grid are (inverted) T-section 60x60x7 mm and angle 60x30x5 mm, respectively. The analytical models are referred to as M1 to M6. The static loading is uniformly applied all over the top-layer area of the grid. The load is gradually increased from zero value up to the failure of the grid. The mechanical properties of concrete and steel are as of Fig. 4. The models assume a non-slip joint condition on the surface of the precast concrete panels with the surface of the top-chord elements.

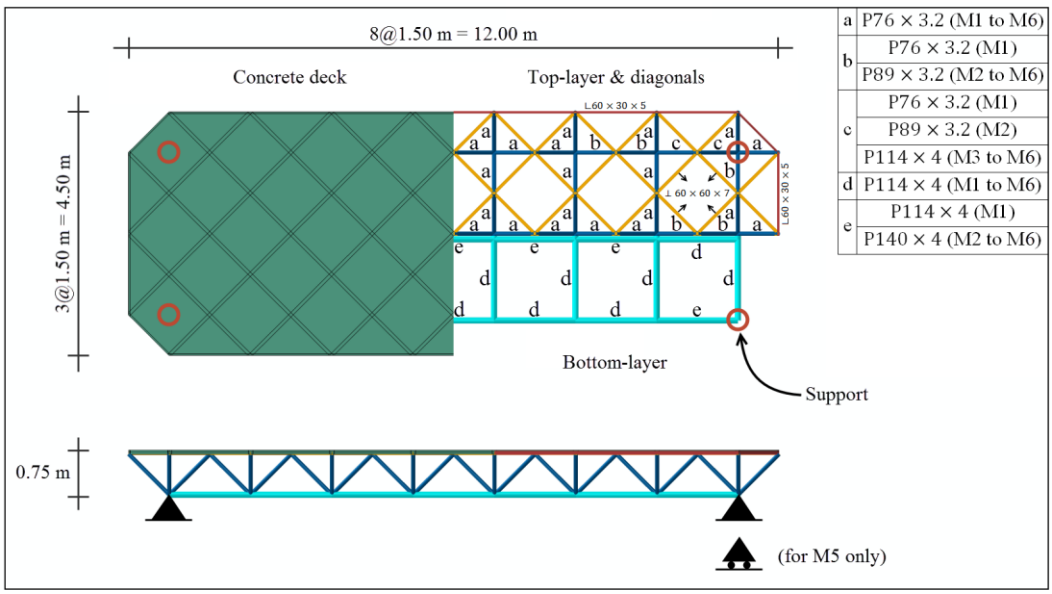

Figure 7. Geometry of the composite double-layer grid models (M1 to M6)

The grid has supports at four corner joints of its bottom-layer. The ratio of the longitudinal to the transversal distances of the supports is (12-2x0.75)/ (4.5-2x0.75) =3.5. Thus, the one-way behaviour of the grids dominates its two-way behaviour. The supports are simple pin-supports for all models, with the exception that, as Fig. 7 shows, for model M5 two of them are roller supports. The table on the right-hand side of Fig. 7 specifies the changes in the cross-sections of the models M1 to M6. According to this table, the frame elements of the grid M2 are stronger than the elements of M1, and elements of M3 are stronger than the elements of M2. The grids M3 to M6 have identical elements.

Figs. 8 to 10 display part of the results of analysis of the models M1 to M6. All the results are presented with respect to a common basis, and therefore are comparable with each other. The quantities under study, correspond to the point of 'incipient collapse' that is, the point (b) of Fig. 11 (as defined by Grigorian, 2014 [4]). The results of each model in Fig. 8 and Fig. 9 have four parts:

- The top-left part of each picture displays the stage of the crack pattern of the concrete deck of the top-layer of the grids, indicated by (PE). The higher (the more positive) value

of PE relates to a more serious (wider and/or deeper) crack. The maximum PE is 0.0542 as the PE colour bar indicates.

- The bottom-left part displays the axial stress, S11 of the reinforcement. A positive S11 relates to a tensile stress. The maximum S11 is 304 MPa and its minimum (= compressive) value is -301 MPa.
- The top-right part displays the axial stress of the top-chords together with the mid-chords of the grid.
- The bottom-right part displays the axial stress of the deformed bottom-chords. The stress S11 of the members of the grid varies in the range of [-366 (compressive), 278 (tensile)] MPa.

The crack patterns of models M1 to M4 show that the borders of the concrete panels that correspond to the position of the top-layer lattice elements are vulnerable to generation of cracks. In grids M1 and M2, a rather large area of the concrete deck is damaged nearby the axis A (and so the axis H). The longitudinal bottom-layer elements of the grid M2 (denoted by (e), in Fig. 7), are stronger than those of the grid M1. Consequently, a stronger composite action develops in M2 than in M1. The intensified cracks of the grid M2 reflect this fact. Similarly, the grid M3, has stronger composite action (and higher crack development) than M2. The compressive post-yielding of the two web elements over the supports accompanies the concrete damage at lines A and H. These two web elements are connected to the supports and are denoted by (b) and (c) in Fig. 7. For grid M1, the compressive stress S11of these two elements has a value well over (-300 MPa), which exceeds the assumed yield stress Fy=240 MPa. As the steel material of Fig. 4 shows, the steel frame elements have identical behaviour in tension and compression. In other words, the numerical models assume that no buckling occurs for the truss elements. Additionally, taking into account the strain hardening of steel (Fig. 4), failure of the grid occurs, in effect, due to the sole failure of the concrete deck. Simultaneously, the four edge-elements of the top chord of the grid (elements B-C and F-G), experience tensile post yielding. At the incipient failure of the grid, the bottom-layer nodes A-2 (and H-2), demonstrate a noticeable horizontal outward displacement along axis 2. The pictures of the web and bottom-layer elements of the grids M1 to M4 reflect this movement. The tensile strength of the concrete material of grid M4 assumes a value identical to its compressive strength, however, it does not noticeably affect the results. The model M6 is a lattice grid that has no concrete deck. The grid M6 acts as the reference grid for evaluation of the increase in strength of the lattice grid due to the composite action.

Fig. 10, shows the relative vertical displacements of grids M1 to M6. The deflection of the grids M1 to M5, due to the composite action has reduced to about ⅓ of the deflection of the lattice grid M6 (which lacks composite action). The grid M5, with roller supports, has about 28% to 37% higher deflection than those of other composite grids.

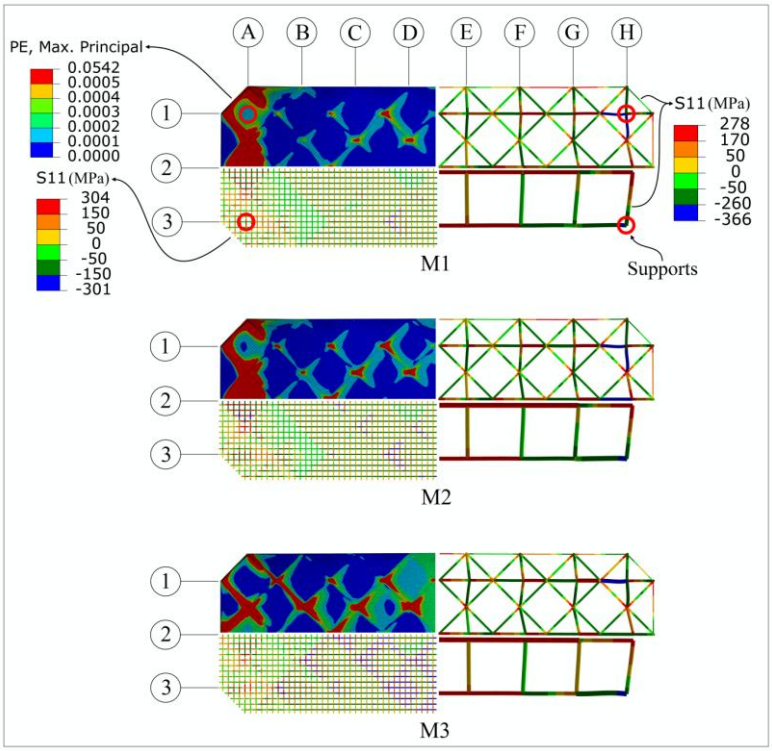

Figure 8. Results of analysis of grids M1 to M3, (for point (b) of Fig. 11)

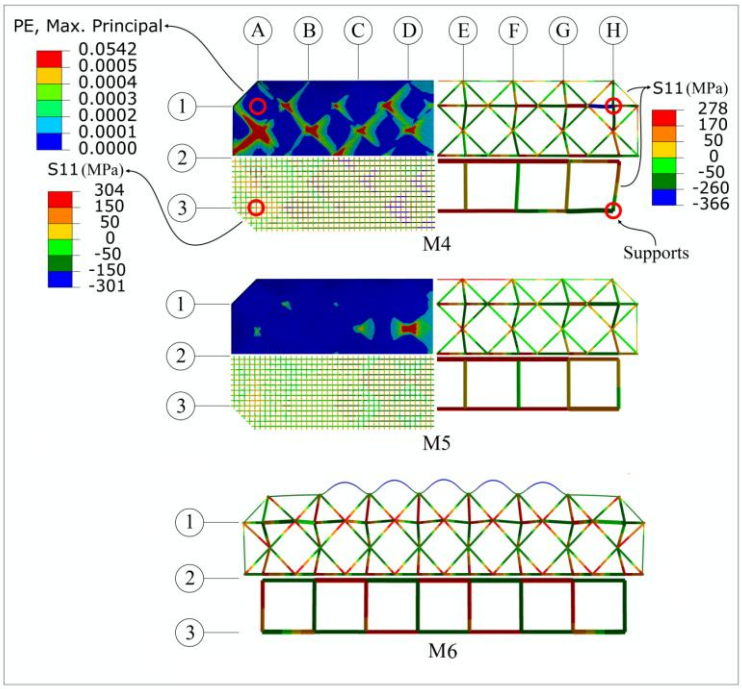

Figure 9. Results of analysis of grids M4 to M6 (for point (b) of Fig. 11)

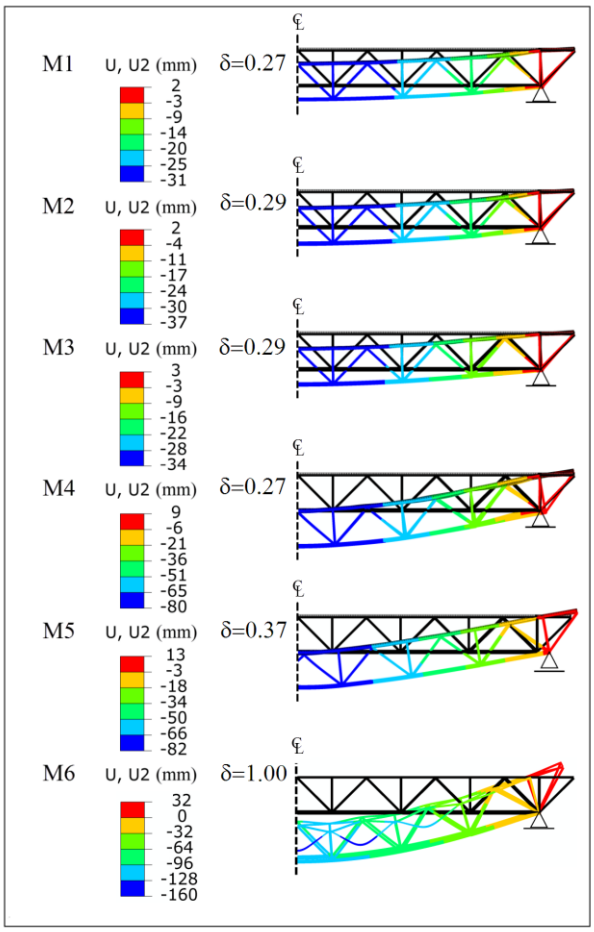

Figure 10. Schematic vertical displacement of the models (for point (b) of Fig. 11)

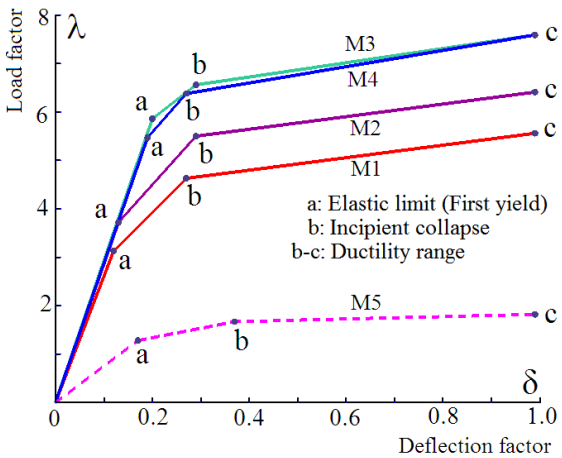

Figure 11. Normalised load-displacement curves for grids

Fig. 11, summarises the normalised load-displacement diagrams for all grids. The graphs are normalised with respect to the results of the reference grid M6 that has no concrete decks. The uniformly distributed load corresponding to point (b) of the reference grid M6, is P_0=231.84 kN. The area covered by the top-layer of the grid is A=51.75 m^2. Thus, the load P_0 is equivalent to a uniformly distributed load q_0= (231.84/51.75)=4.48 kN/m^2. The (maximum) vertical displacement corresponding to P_0 is Δ_0=115.8 mm (point (b) of grid M6). The vertical axis of the diagrams of Fig. 11, is λ (=P/P_0), and its horizontal axis is δ (=Δ/Δ_0). They indicate the normalised load and displacement of the composite grids. At points (a) the elastic region of the grids terminate. The comparison of the elastic limit (that is, the point (a) of the graphs) of various grids shows that:

λa= {3.13, 3.72, 5.86, 5.47, 1.28}, and

δa= {0.12, 0.13, 0.2, 0.19, 0.17}.

Then, a measure of the stiffness of the grids will be:

ka= ($\lambda a/\delta a$) = {26.1, 28.6, 29.3, 28.8, 7.5}.

Thus, the grids M1 to M4 have a higher stiffness than the grids M5, which with a value of 7.5 has the lowest stiffness. Hence, the introduction of roller supports has reduced the stiffness of the composite grid by factor of 3.5 to 3.9.

For the point (b), we have

λb= {4.63, 5.50, 6.56, 6.38, 1.67}, and

δb= {0.27, 0.29, 0.29, 0.27, 0.37}.

And a measure of the stiffness of the grids for the incipient collapse zone is:

kb= (λb-λa)/(δb-δa) = {10, 11.1, 7.8, 11.4, 2}.

Finally, for the point (c), we have

λc= {5.56, 6.41, 7.59, 7.59, 1.82}, and

δc= {0.99, 0.99, 0.99, 0.99, 1}.

And the stiffness of the grids at the ductility range is:

kc= (λc-λb)/(δc-δb) = {1.3, 1.3, 1.5, 1.7, 0.2}.

The stiffness of the grid considering the load P_0 and the deflection Δ_0 will be k_0=P_0/Δ_0=231.84/115.8=2.0 kN/mm. Taking into account k_0, the stiffness of kc for grid M3 at the ductility range, will be kc=3.0 kN/mm. The mean value of the relative elastic stiffness of the grids M1 to M4 is S_e=28.2, which reduces to S_y=0.36S_e in the post-yield and prior to incipient collapse. At the ductility range the stiffness has the value S_d=0.05S_e.

The composite grids M3 and M4 have the highest strength among all the composite grids and their load-displacement character are almost identical. The incipient collapse displacements of the composite grids M1 to M4 are almost equal, but that of the grid M5, which has roller supports, is about 30% higher. The displacement breadth of the grids M3 and M4 between the elastic limit and the incipient collapse [a, b], are about half of those of the grids M1 and M2. Up to elastic limit, the composite grid can carry about 200% to 450% more load than the corresponding lattice grid. Even though, the grid M5 has roller supports, it has about 28% higher load capacity than the lattice grid M6, with all pinned supports. At the same time, a composite grid with (roller + pin) supports has about 20% of the load capacity of the identical grid with (pin + pin) supports.

4. CONCLUDING REMARKS

In many applications with heavy loads, concrete is a suitable cover for single-layer and double-layer lattice steel grids. Subject to certain provisions, the concrete decks, which cover the grids, can develop the steel-concrete composite action as well. The present paper, studies the effect of concrete decks in increasing the strength and stiffness of simply supported double-layer grids. Firstly, the load capacity of a concrete panel was determined under various boundary conditions. Then, the variation in the load capacity of composite double-layer grids under various conditions was obtained. The suggested details presumes precast concrete panels, however, the results are equally applicable for in situ concrete decking with the same geometry and details. It is essential to carry out a number of load tests on double-layer grids, in order to validate the extent of the applicability of the numerical results and to evaluate the difference in the load capacity of the precast and in situ concrete decking. The paper shows that the combined and composite action of concrete decks with a lattice double-layer grid would increase its load capacity up to 5 times. However, a global evaluation of the strength of a composite double-layer grid depends on the load capacity of its constituent concrete panels as well.

Acknowledgements: The composite double-layer grid and the test mentioned in Fig. 1, is a mock-up for a number of projects realised by SAFIRA Company of Iran, while the second author was a participant of that company. Also, the authors gratefully acknowledge the help of Pouyan Pourakbar for numerical modelling.

REFERENCES

1. Ban H, Bradford MA. Elastoplastic cross-sectional behavior of composite beams with high-strength steel: analytical modeling, *Journal of Structural Engineering*, Issue 10, **141**(2015), DOI: 10.1061/(ASCE)ST.1943-541X.0001208.
2. Grigorian M. Performance control for efficient design of regular grillages under uniform loading, *Asian Journal of Civil Engineering (BHRC)*, No. 3, **14**(2013) 429-44.
3. Grigorian M. A new approach to plastic design and optimization of parallel chord vierendeel girders, *International Journal of Optimization in Civil Engineering*, No. 3, **3**(2013) 371-88.
4. Grigorian M. Performance control for efficient design of double-layer grids under uniform loading, *International Journal of Advanced Structural Engineering*, No. 52, **6**(2014), DOI10.1007/s40091-014-0052-7.
5. Kaveh A, Bakhshpoori T and Afshari E. An optimization-based comparative study of double-layer grids with two different configurations using cuckoo search algorithm, *International Journal of Optimization in Civil Engineering*, No. 4, **1**(211) 507-20.
6. Kaveh A, Hassani M. Ant colony algorithms for nonlinear analysis and optimal design of structures, *International Journal of Optimization in Civil Engineering*, No. 4, **1**(2011) 571-95.
7. Gholizadeh S, Torkzadeh P, Jabarzadeh S. Optimum shape design of double-layer grids

by quantum behaved particle swarm optimization and neural networks, *International Journal of Optimization in Civil Engineering*, No. 1, **3**(2013) 85-98.

8. Gholizadeh S, Sheidaii M R and Farajzadeh. Seismic design of double-layer grids by neural networks, *International Journal of Optimization in Civil Engineering*, No. 1, 2(2012) 29-45.
9. Lan TT. Recent trends and developments of space structures in china, *Proceedings of 3rd International Conference on Space Structures*, Edited by H Nooshin, Elsevier Applied Science Publishers, 1984, ISBN 13: 9780853343097.
10. Shilin D, Hengxi X. Development and application of the composite space truss in china, *Proceedings of the 4th Conference on Space Structures, University of Surrey*, pp. 1572-1580, Editors GAR Parke, Howard CM, Thomas Telford, London 1993, DOI: 10.1680/ss4v1.19683.
11. Liu XL. Development of grid structures in china, *Journal of the International Association for Shell and Spatial Structures*, Special issue for recent spatial structures in China, No. 2, **47**(2006) 101-10.
12. Dong S, Zhao Y. 34 types of space structures: classification and practical application in China, *International Symposium, New Olympics New Shell and Spatial Structures*, October 16-19, 2006, Beijing, China.
13. El-Sheikh A. New space truss system-from concept to implementation, *International Journal of Engineering Structures*, Issue 9, **22**(2000) 1070-86.
14. Schaad JA. Two-way steel floor system using open-web joists, Msc Thesis, Milwaukee, Wisconsin, 2005.
15. Heristchian M. Space structures with composite sections and a stadium roof, *Symposium on the Application of Steel Structures in Construction in the World and the Introduction in Turkey*, 22-23 March 1990, Ankara, Turkey.
16. Schlaich J, Bergemann R. Light Structures, Edited by Bögle A, Schmal PC, Flagge I, Prestel München, Germany, ISBN: 9783791329185, 2003.
17. Strasky J. Pedestrain bridges utilising high strength concrete, *International Journal of Space Structures*, No. 1, **22**(2007) 61-79.
18. Hong SC. Analysis and experiment of composite space slab-grid structure, *Proceedings of the 3rd International Conference on Space Structures*, pp. 192-195, Edited by H Nooshin, 1984, Elsevier Applied Science Publishers, ISBN 13: 9780853343097.
19. Thomson KW, Kubik LA. Development and testing of the CUBIC composite floor, *Proceedings of the 4th Conference on Space Structures*, University of Surrey, pp. 1510-1517, Editors GAR Parke, Howard CM, Thomas Telford, London 1993, DOI: 10.1680/ss4v1.19683.
20. EL-Sheikh AI, McConnel RE. Experimental study of behavior of composite space trusses, *Journal of Structural Engineering*, **119**(1993) 747-66.
21. EL-Sheikh AI, El-Bakry H. Experimental study of behavior of new space truss system, *Journal of Structural Engineering*, **122**(1996) 845-53.
22. El-Sheikh AI. Optimum design of composite space trusses, *Journal of the International Association for Shell and Spatial Structures*, *IASS*, No. 130, **40**(1999).
23. Appendix 2: Code of Practice 400: Lattice Steel Spatial Structures, Technical Bureau of Management and Planning Organisation of Iran, 2010.

24. Park R, Paulay T. Reinforced concrete structures, New York, Wiley & Sons, 1975.
25. Wahalathantri BL, Thambiratnam DP, Chan THT, Fawzia S. A Material model for flexural crack simulation in reinforced concrete elements using Abaqus, *Proceedings of the First International Conference on Engineering, Designing and Developing the Built Environment for Sustainable Wellbeing*, Queensland University of Technology, Brisbane, Qld, 2011, pp. 260-264.
26. Abaqus Analysis User Manual – Abaqus Version 6.14-1, 2014.